Turkish Journal of Physics

http://journals.tubitak.gov.tr/physics/

Invited Review Article

Turk J Phys
(2014) 38: 391 – 398

doi:10.3906/fiz-1405-12

Morphology and crystallinity control of wet chemically grown ZnO nanorods

János VOLK[1,2,*], **Róbert ERDÉLYI**[1]

[1]Research Centre for Natural Sciences, Institute for Technical Physics and Materials Science, Hungarian Academy of Sciences, Budapest, Hungary

[2]Department of Electrical and Computer Engineering, Virginia Commonwealth University, Richmond, Virginia, USA

Received: 20.05.2014 • **Accepted:** 03.06.2014 • **Published Online:** 10.11.2014 • **Printed:** 28.11.2014

Abstract: The controlled growth of ZnO nanorods on technologically relevant substrates is essential for their practical integration into next generation optoelectronic and piezoelectric devices. In this report, highly ordered and uniform vertical ZnO nanorod arrays were synthesized using a facile, low temperature selective area wet chemical growth process. The nanorods were grown through nucleation windows that were patterned in a PMMA mask using electron beam lithography. At first, the technique was demonstrated on 'ideal' ZnO single crystal substrates, where the geometrical parameters of the highly uniform and crystallographically coherent nanorods were dictated by the nucleation pattern, the polarity of the substrate, and the growth conditions. The obtained geometry was then compared to 4 further arrays corresponding to different ZnO seed layers deposited on Si and sapphire substrates. Scanning electron microscopy showed that the crystal orientation and the alignment of the nanorods were determined by the underlying seed layer. The piezoresponse force microscopy revealed that the d_{33} piezoelectric tensor component of the wet chemically grown nanorods was comparable (6–12 pm/V) to that of the highest value measured on ZnO single crystal (12.4 pm/V). The presented nanorod arrays have several potential applications, from nanorod based light emitting devices to CMOS compatible piezoelectric nanoforce sensors.

Key words: ZnO nanorod, aqueous chemical growth, piezoresponse force microscopy

1. Introduction

Between the beginning of the millennium and 2013, the research interest in quasi one dimensional ZnO crystals such as nanowires (NWs) and nanorods (NRs) continuously grew each year, as indicated by the number of published scientific papers. At the beginning, investigations were mainly focused on their interesting optical properties and UV light emission [1], which were later extended to include the exploration of electrical [2], mechanical [3,4], and coupled electromechanical properties [5]. Besides this progress, several synthesis methods have also been demonstrated, among which are high temperature physical vapor deposition [6], vapor-liquid-solid [7,8], metal–organic chemical vapor deposition (MOCVD) [9–11], pulsed laser deposition [12], and low temperature aqueous chemical growth techniques [13,14]. Several potential applications have also been demonstrated, such as UV light-emitting diodes [15,16], UV lasers [17] and photodetectors [18], nanopillar lenses [19], dye sensitized solar cells [20], and electromechanical force/tactile sensors [21].

Despite the above mentioned enormous research and great potential of ZnO nanostructures, their intro-

*Correspondence: volk@mfa.kfki.hu

duction into optoelectronic or microelectronic products has not been attained yet. One of the major obstacles, similar to ZnO thin films, is the lack of stable p-type doping. The other technological challenge is related to the integration of tiny ZnO building blocks into conventional Si or sapphire substrate based microelectronic devices. For Si CMOS technology the allowed temperature is limited to around 400 °C after metallization, excluding high temperature dry chemical NW synthesis. Moreover, the integration of ZnO NWs in the existing semiconductor technology requires excellent geometrical uniformity, precise position and alignment control, and high packing density. Selective area wet chemical grown (SAWCG) vertical ZnO NRs have great potential to fulfill all of these requirements. Here we summarize our efforts toward the growth of position controlled vertical ZnO NR arrays on different substrates ranging from ZnO single crystal as ideal homoepitaxial template to more economical ZnO coated sapphire and Si substrates. The compared structures are promising for various novel optoelectronic and integrated piezoelectric sensor devices.

Moreover, a highly conductive seed layer beneath the NR enables the accurate piezoelectric investigation of individual ZnO nanocrystals by minimizing the serial resistance of the template. Section 4 describes the results of piezoresponse force microscopy carried out on NRs grown on a highly conductive Pt/ZnO template.

2. Selective area wet chemical growth of ZnO nanorods

Highly uniform SAWCG NR arrays were first realized on Zn-polar (0001) and O-polar ($000\bar{1}$) ZnO single crystals (supplied by Furuuchi Chemicals). The process flow for the fabrication of the ZnO NRs is shown in Figure 1 and reported in [22]. Each seed surface was first washed ultrasonically in acetone, ethanol, and deionized water (Figure 1a). In order to provide patterned templates for subsequent NR growth, a $\sim$250 nm thick poly(methyl methacrylate) (PMMA) resist layer was spin coated onto each seed surface, and a regular triangular or honeycomb lattice was exposed using the Elionix 7500 or JEOL IC 848-2 electron beam lithography system (Figure 1b). The patterned area of 150 μm $\times$ 150 μm consists of circular growth windows with a diameter of about 120–130 nm, while the center-to-center distance was in the range of Λ = 250–500 nm. The ZnO NR arrays were synthesized at 85–95 °C for 0.5–3.5 h in an aqueous solution of zinc nitrate hexahydrate ($Zn(NO_3)_2{\cdot}6H_2O$) (4 mM) and hexamethylene tetramine ($(CH_2)_6N_4$) (4 mM) (Figure 1c). The specimen was mounted upside-down on a polytetrafluoroethylene sample holder in order to prevent any precipitates that formed in the nutrient solution from falling onto the substrates (which would have inhibited the growth of the NRs). After the synthesis process, the PMMA layer was removed in acetone and the specimens were thoroughly rinsed with deionized water (Figure 1d).

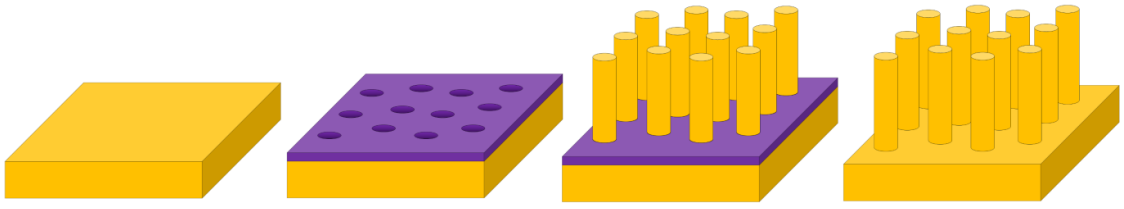

Figure 1. Schematic process flow of ZnO NR array growth. The fabrication steps are: surface treatment of ZnO seed surface **(a)**, pattern generation in PMMA by e-beam lithography **(b)**, aqueous chemical growth of NRs **(c)**, and PMMA removal **(d)**.

The scanning electron microscopy (SEM, Zeiss 1540XB) image in Figure 2a shows an excellent geometrical uniformity of the NRs, which are aligned normal to the surface. The SEM image taken on some intentionally

fractured NRs in Figure 2b reveals a hexagonal prism shaped upper part surrounded by nonpolar $\{1\bar{1}00\}$ faces and a $\sim$250 nm long cylindrical lower segment that appears to have been formed in the nucleation window of the PMMA layer. Beyond the c-axis alignment, the wurtzite type NRs show a coherent in-plane orientation as well, which was dictated by the crystal orientation of the single crystal ZnO as seen in Figure 2c. We have found that by changing the hole diameter in the PMMA and the growth time, the diameter and the length of the NRs can be tuned in the $\sim$90–250 nm and $\sim$0.5–3.5 μm ranges, respectively. The polarity of the NRs can also be controlled by growing on either the Zn- or O-polar surface of the c-plane ZnO. Zn-polar growth is accompanied with a somewhat lower growth rate compared to the O-polar case and a less tapered NR geometry as reported by Gautam et al. [23]. In case of insufficient spacing between the nucleation windows on O-polar ZnO crystal, the notable lateral growth can also result in coalescence of the crystals and formation of a continuous layer as seen in Figure 2d. In contrast to the Zn-polar surface, well separated slightly tapered NRs were grown (Figure 2c) on the O-polar surface.

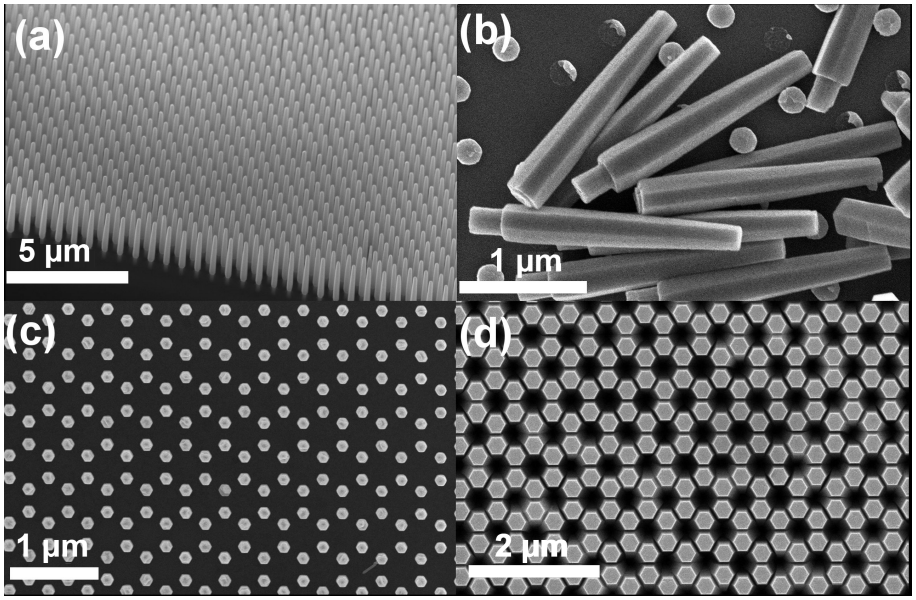

Figure 2. SEM image of ZnO nanostructures grown by selective area wet chemical process onto ZnO single crystal. Tilt view image of all-ZnO NR arrays showing excellent uniformity and c-axis alignment **(a)**. The NRs are built up from a hexagonal prism shaped upper segment and a $\sim$250 nm cylindrical shaft, which was developed in the nucleation window of the PMMA layer as shown on the fractured NRs **(b)**. Top view image of well separated nanorods on Zn-polar surface **(c)** compared to a coalesced layer on O-polar ZnO single crystal **(d)**.

It is worth noting that the diameter of the NRs is limited by the resolution of electron beam lithography and not by the wet chemical growth process. For instance, by means of atomic force microscopy lithography, the hole diameter in the thin PMMA layer and thus the diameter of the grown NR can be downsized to 30 nm as reported by Volk et al. [24].

Although, as it was shown above, SAWCG on single crystal ensures excellent crystallographic alignment and geometry control, to make the synthesis compatible with the existing CMOS and compound semiconductor technologies it has to be adapted to less expensive Si and sapphire substrates. Hence, in the next section, the effects of the substrate and seed layer covering it are addressed.

3. The effect of seed layer

After unsuccessful attempts of SAWCG directly on different surfaces including Si(111), glass, Si_3N_4, thermal SiO_2, GaN, sapphire, and Al, we concluded that a proper seed layer is a necessary requirement for aqueous wet chemical growth. Until now, we have found only ZnO as a proper seed layer, but we cannot exclude other candidates that may come along, e.g. those with lattice matching and thermodynamically favorable surfaces. In the following, we compare the previously described all-ZnO nanorod arrays (denoted as 'Bulk') with 4 different ZnO seed layers.

The first ZnO seed layer investigated was grown by atomic layer deposition (ALD) on a relatively thick ($\sim$6 μm) epitaxial MOCVD GaN film (TDI Corporation) on c-sapphire (denoted as 'ALD/GaN'). The seed layer was grown with 500 ALD cycles at 300 °C deposition temperature as reported by Baji et al. [25].

The second layer variety, a highly Ga doped ZnO layer (denoted as 'MBE/sap') was deposited by an SVT Associates molecular beam epitaxy (MBE) system equipped with a commercial plasma O-source by Addon. After deposition of a thin low temperature undoped ZnO nucleation layer, Zn and Ga effusion cells were employed and set to 350 °C and 600 °C, respectively, to grow the highly Ga doped ZnO layer. During growth, the substrate temperature was 400 °C at an oxygen pressure of 3.7×10^{-6} Torr [26].

The third ZnO seed layer variety was grown by pulsed laser deposition (PLD) onto Si(111) wafer (denoted as 'PLD/Si') using a KrF excimer laser (248 nm) [27]. The fourth and last seed layer investigated was grown on a Si(100) wafer in Ar/O_2 atmosphere by DC reactive magnetron sputtering of an Al doped (2 wt.%) Zn target (denoted as 'Sputt/Si'). In order to stabilize the glow discharge, a pulse signal was added to the direct current voltage. The deposition was carried out without bias or substrate preheating [28]. It should be noted that no attempt was made to remove the native amorphous SiO_2 passivation layer from Si substrates of PLD/Si and Sputt/Si. The parameters of the compared seed layer are summarized in the Table.

Table. Comparison of the seed layers.

Sample	Substrate	Deposition temperature [°C]	Layer thickness [nm]	RMS roughness [nm]	Crystal structure	Specific resistance [Ω cm]
Bulk	ZnO (0001)	-	-	0.13	Single crystal	1.5×10^{2}
ALD/GaN	GaN/AlN/c-sapphire	300	32	0.10	Epitaxial	5.4×10^{-1}
MBE/sap	a-sapphire	400	375	0.69	Epitaxial	2.6×10^{-4}
PLD/Si	Si (111)	500	427	0.98	Highly textured	4.19×10^{-1}
Sputt/Si	Si (100)	RT	155	1.66	Textured	4.14×10^{-3}

Before nanostructure growth, the surface of the substrates was studied by atomic force microscopy (AFM) in semicontact mode (AIST-NT, SmartSPM 1010). The same SAWCG growth was carried out on each seed layer as described above with a triangular lattice (Λ = 500 nm) of growth windows, at a growth temperature of 85 °C and growth time of 3.5 h. The only exception was the MBE/sap seed case where the diameter of the windows on the seed was 200 nm in contrast to 120 nm used for other seed layers.

The SEM images in Figures 3a–3j show that while all the growth experiments resulted in regular arrays of NRs with $\sim$2 μm length and 100–300 nm diameter, depending on the seed layer they have different NR morphologies and orientations. The NRs grown on the Bulk (Figure 3a and 3f), ALD/GaN (Figure 3b and 3g), MBE/sap (Figures 3c and 3h), and PLD/Si (Figures 3d and 3i) were aligned normal to the surface, while

those on Sputt/Si (Figures 3e and 3j) exhibited a greater dispersion in their orientation. Moreover, the NRs grown on the Bulk, the ALD/GaN, and the MBA/sap showed a common relative orientation of their hexagonal crystal facets on the surface (Figures 3a–3c). Closer observation of the NR grown on the Sputt/Si (Figures 3e and 3j) and PLD/Si (Figures 3d and 3i) also revealed that, in some cases, multiple NRs grew in a given growth window.

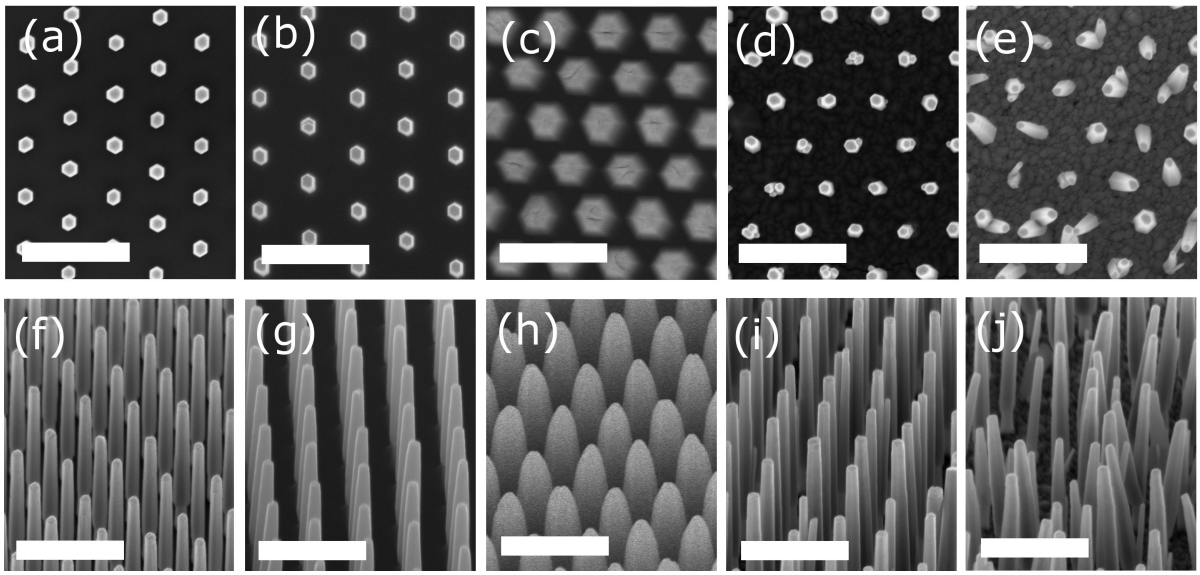

Figure 3. Top view (upper row) and tilted view (lower row) scanning electron micrographs of vertical ZnO NRs grown on different substrates (the length of the white scale bar is 1 μm): ZnO single crystal **(a and f)**; ALD deposited ZnO on GaN/c-Al_2O_3(0001) **(b and g)**; MBE deposited Ga:ZnO on c-Al_2O_3(0001) **(c and h)**; PLD deposited ZnO on Si(111) **(d and i)**; and reactive magnetron sputtered ZnO on Si(100) **(e and j)**.

The AFM images of Figures 4a–4e suggest that the PLD/Si (Figure 4d) and Sputt/Si (Figure 4e) seed layers are composed of tiny crystals where the grains appear to range from several tens of nanometers up to hundred nanometers in diameter. This grain size range can explain the presence of multiple NRs on the PLD/Si and Sputt/Si seed layers, since they are comparable to or lower than the diameter of the e-beam lithography patterned growth windows. Thus, it is very likely that more than one grain in the seed layer can nucleate in a single growth window. The Bulk, ALD/GaN, and MBE/sap substrates have significantly smoother surfaces (Table) and larger grain sizes (Figures 4a–4c). This could explain the common relative orientation of the NR hexagonal crystal facets as the result of epitaxial growth of the NRs on grains large enough to include many growth windows. It can therefore be concluded that the alignment and crystal orientation of the ZnO NRs is determined by the local crystal quality of the seed layer. This finding is in good agreement with the quantitative XRD results of Erdélyi et al. [29].

4. Piezoresponse measurements

For the piezoelectronic investigation, a dedicated ZnO NR array was grown on a highly conductive (2.3 Ω/sq) c-axis textured ZnO/Pt (220 nm/100 nm) double layer coated c-sapphire. Further details about the template can be found in the work of Kim et al. [30]. The grown NRs showed good c-axis alignment and polycrystalline nature (Figure 5a), which can be ascribed to the uniaxial texture of the (111) Pt layer. In order to avoid the

fracture of the NRs in contact mode AFM scanning they were infiltrated by spin coated photoresist and partly etched back in oxygen plasma to make their tips accessible for the scanning probe.

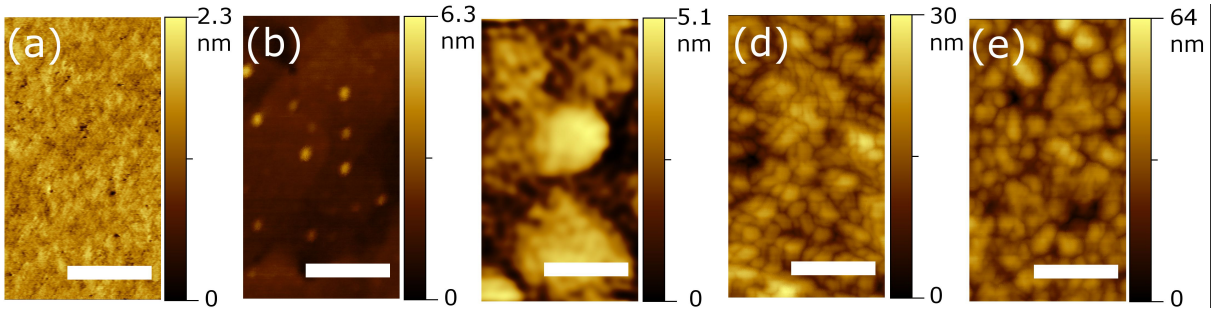

Figure 4. AFM images of ZnO seed surfaces (the length of the white scale bar is 200 nm): ZnO single crystal **(a)**; ALD deposited ZnO on GaN/c-Al_2O_3(0001) **(b)**; MBE deposited Ga:ZnO on c-Al_2O_3(0001) **(c)**; PLD deposited ZnO on Si(111) **(d)**; reactive magnetron sputtered ZnO on Si(100) **(e)**.

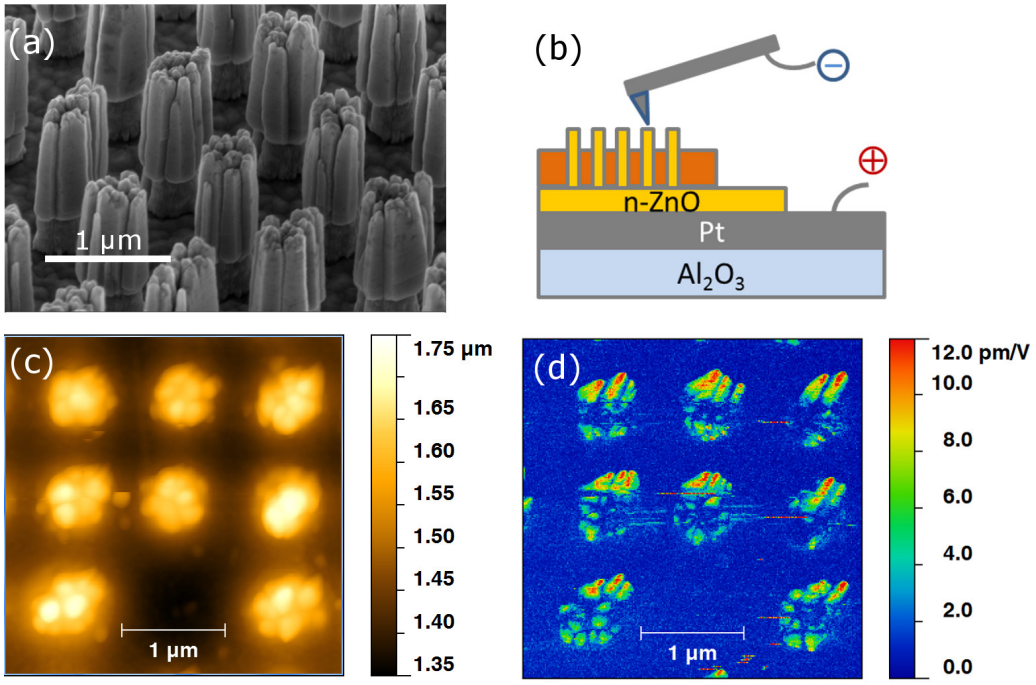

Figure 5. SEM image of the polycrystalline ZnO nanorods grown on ZnO/Pt/c-sapphire template **(a)**. Schematics of piezoresponse scanning probe measurement **(b)**. In order to avoid the fracture of the wet chemically grown crystals, the array was infiltrated by photoresist and etched back partially. The measured contact mode height **(c)** and the corresponding piezoresponse map **(d)**.

The piezoelectric activity of individual NRs was characterized by piezoresponse atomic force microscopy, where the mechanical response of the investigated material is recorded on an alternating voltage signal (Figure 5b). A SmartSPM 1010 (AIST NT) multimode scanning probe microscope mounted with a conductive AFM tip was used for an excitation signal (52 kHz, 6 V). In order to determine the d_{33} constant of the piezoelectronic tensor represented by a 3 $\times$ 6 matrix in Voigt notation for the NR, the major part of the applied voltage has to drop across the NR, which necessitates that the resistance of the substrate is minimized.

The obtained height (Figure 5c) and the corresponding piezoresponse (Figure 5d) image show that the maximal piezoresponse values were obtained at the tip of the nanorods. The calculated d_{33} values of the piezoelectronic tensor were in the 6–12 pm/V range. These values are similar to the results reported by Scrymgeour et al. [31] and close to the bulk value (12.4 pm/V) obtained for Li compensated highly resistive ($>10^8\Omega$cm) ZnO crystals [32], which can be regarded as the maximal experimental value for ZnO.

5. Conclusions

Highly regular ZnO nanocrystal arrays were grown on various seed layers and substrates using a low temperature, selective area wet chemical growth method. The geometry of the NRs and their relative alignment in the array were found to be defined by the seed window and by the growth conditions, while their alignment and crystal properties were determined by the crystalline properties of the ZnO seed layer. Although rather expensive electron beam lithography was used in this particular study to pattern the mask layer, the technique can be easily adapted to other more productive and less expensive methods such as nanoimprint lithography [33], laser interference lithography [34], and nanosphere photolithography [35].

Well oriented NR arrays grown on highly transparent and highly conductive GZO epitaxial layers have great potential in several nanophotonic applications such as nanorod LED or laser cavity pending the availability of stable p-type doping of ZnO NRs. On the other hand, they can also be used as passive optical elements, e.g., to facilitate top surface light extraction from conventional InGaN/GaN and AlGaN/GaN multiple quantum well blue and UV LEDs.

The c-axis oriented nanocrystals, which were grown on Si coated by PLD ZnO, can provide new functionalities for CMOS based hybrid electronic and sensor devices. However, a highly textured layer on lattice mismatched substrates like Si needs a higher deposition temperature ($\sim$500 °C) than those on lattice matched substrates, as indicated in the Table. This growth temperature is often intolerable for Si technology after metallization and this problem remains to be solved in the future.

As was pointed out by piezoresponse force microscopy, the wet chemically grown NRs showed relatively high piezoelectric constants (6–12 pm/V), which bodes well for nanomechanical sensors and energy harvesting devices. However, these novel NR based devices still face several challenges, such as the compensation of free carriers and proper metallization schemes for vertical NRs.

Acknowledgments

This work was supported by a PiezoMAT ("High-resolution fingerprint sensing with vertical piezoelectric nanowire MATrices") FP7 small- or medium-scale focused research grant. JV acknowledges the support of the Hungarian-American Enterprise Scholarship Fund (HAESF).

References

[1] Huang, M. H.; Mao, S.; Feick, H.; Yan, H.; Wu, Y.; Kinde, H.; Weber, E.; Russo, R.; Yang, P. *Science* **2001**, *292*, 1897–1899.

[2] Schlenker, E.; Bakin, A.; Weimann, T.; Hinze, P; Weber, D. H.; Golzhauser, A.; Wehmann, H.; Waag, A. *Nanotechnology* **2008**, *19*, 365707.

[3] Hoffmann, S.; Östlund, F.; Michler, J.; Fan, H. J.; Zacharias, M.; Christiansen, S. H.; Ballif, C. *Nanotechnology* **2007**, *18*, 205503.

[4] Erdélyi, R.; Madsen, H. M.; Sáfrán, G.; Hajnal, Z.; Lukacs, I. E.; Fülöp, G.; Csonka, S.; Nygard, J; Volk, J. *Sol. Stat. Comm.*, **2012**, *152*, 1829–1833.

[5] Wang, X.; Zhou, J.; Song, J.; Liu, J.; Xu, N.; Wang, Z. L. *Nano Lett.* **2006**, *6*, 2768–2772.

[6] Li, J; Zhang, Q.; Peng, H; Everitt, H. O.; Qin, L.; Liu, J. *J. Phys. Chem. C* **2009**, *113*, 3950–3954.

[7] Huang, M. H.; Wu, Y.; Feick, H.; Tran, N.; Weber, E.; Yang, P. *Adv. Mater.* **2001**, *13*, 113–116.

[8] Yao, B. D.; Chan, Y. F.; Wang, N. *Appl. Phys. Lett.* **2002**, *81*, 757–759.

[9] Park, W. I.; Yi, G. C.; Kim, M. Y.; Pennycook, S. J. *Adv. Mater.* **2002**, *14*, 1841–1843.

[10] Park, W. I.; Kim, D. H.; Jung, S. W.; Yi, G. C. *Appl. Phys. Lett.* **2002**, *80*, 4232–4234.

[11] Yuan, H.; Zhang, Y. J. *Cryst. Growth Des.* **2004**, *263*, 119–124.

[12] Sun, Y.; Fuge, G. M.; Ashfold, M. N. R. *Chem. Phys. Lett.* **2004**, *396*, 21–26.

[13] Verges, M. A.; Mifsud, A.; Serna, C. J. *J. Chem. Soc. Faraday Trans.* **1990**, *86*, 959–963.

[14] Vayssieres, L.; Keis, K.; Lindquist, S. E.; Hagfeldt, A. *J. Phys. Chem. B* **2001**, *105*, 3350–3352.

[15] Park, W. I.; Yi, G. C. *Adv. Mater.* **2004**, *16*, 87–90.

[16] Chen, M. T.; Lu, M. P.; Wu, Y. J.; Song, J.; Lee, C. Y.; Lu, M. Y.; Chang, Y.C.; Chou, L. J.; Wang, Z. L.; Chen, L. J. *Nano Lett.* **2010**, *10*, 4387–4393.

[17] Chu, S.; Wang, G.; Zhou, W.; Lin, Y.; Chernyak, L.; Zhao, J.; Kong, J.; Li, L.; Ren, J.; Liu, J. *Nat. Nanotechnol.* **2011**, *6*, 506–510.

[18] Wang, G.; Chu, S.; Zhan, N.; Lin, Y.; Chernyak, L.; Liu, J. *Appl. Phys. Lett.* **2011**, *98*, 041107.

[19] Volk, J.; Hakansson, A.; Miyazaki, H. T.; Nagata, T.; Shimizu, J.; Chikyow, T. *Appl. Phys. Lett.* **2008**, *86*, 054102.

[20] Law, M.; Greene, L. E.; Johnson, J. C.; Saykally, R.; Yang, P. D. *Nat. Mater.* **2005**, *4*, 455–459.

[21] Wu, W; Wen, X; Wang, Z. L. *Science* **2013**, *340*, 952–957.

[22] Volk, J.; Nagata, T.; Erdélyi, R.; Bársony, I.; Tóth, A. L.; Lukács, I. E.; Czigány, Z.; Tomimoto, H.; Shingaya, Y.; Chikyow, T. *Nanoscale Res. Lett.* **2009**, *4*, 699–704.

[23] Gautam, U. K.; Imura, M.; Rout, C. S.; Bando, Y.; Fang, X.; Dierre, B.; Sakharov, L.; Govindaraj, A.; Sekiguchi, T.; Golberg, D.; et al. *P. Am. Acad. Arts Sci.* **2010**, *107*, 13588–13592.

[24] Volk, J.; Szabó, Z.; Erdélyi, R.; Khánh N. Q. In: *Oxide-Based Materials and Devices III, Proceedings of SPIE - The International Society for Optical Engineering*; Teherani FH, Look DC, Rogers DJ, Eds. SPIE: Bellingham, WA, USA, 2012.

[25] Baji, Z.; Labadi, Z.; Horvath, Z. E.; Molnar, G.; Volk, J.; Barsony, I.; Barna, P. *Cryst. Growth Des.* **2012**, *12*, 5615–5620.

[26] Liu, H. Y.; Avrutin, V.; Izyumskaya, N.; Özgür, Ü.; Yankovich, A. B.; Kvit, A. V.; Voyles, P. M., Morkoç, H. *J. Appl. Phys.* **2012**, *111*, 103713.

[27] Rogers, D. J.; Teherani, F. H.; Ougazzaden, A.; Gautier, S.; Divay, L.; Lusson, A.; Durand, O.; Wyczisk, F.; Garry, G.; Monteiro, T.; et al. *Appl. Phys. Lett.* **2007**, *91*, 071120.

[28] Németh, Á.; Major, C.; Fried, M.; Lábadi, Z.; Bársony, I. *Thin Solid Films* **2008**, *516*, 7016–7020.

[29] Erdélyi, R; Nagata, T; Rogers, D. J.; Teherani, F. H.; Horvath, Z. E.; Labadi, Z.; Baji, Z; Wakayama, Y; Volk, J. *Cryst. Gr. Des.* **2011**, *11*, 2515–2519.

[30] Kim, T.; Yoshitake, M.; Yagyu, S.; Nemsak, S.; Nagata, T.; Chikyow, T. *Surf. Interface Anal.* **2010**, *42*, 1528–1531.

[31] Scrymgeour, D. A.; Hsu, J. W. P. *Nano Lett.* **2008**, *8*, 2204–2209.

[32] Crisler, D. F.; Cupal, J. J.; Moore, A. R. *Proc. IEEE* **1968**, *56*, 225–226.

[33] Oh, S.; Nagata, T.; Volk, J.; Wakayama, Y. *Appl. Phys. Exp.* **2012**, *5*, 095003.

[34] Wei, Y.; Wu, W.; Guo, R.; Yuan, D.; Das, S.; Wang, Z. L. *Nano Lett.* **2010**, *10*, 3414–3419.

[35] Szabo, Z.; Volk, J.; Fülöp, E.; Deák, A.; Bársony, I. *Phot. Nano. Fund. Appl.* **2013**, *11*, 1–7.